RFI ANALYSIS IN SMOS IMAGERY

Adriano Camps[1], *Jérôme Gourrion*[2], *José Miguel Tarongí*[1],
Antonio Gutiérrez[3], *Jose Barbosa*[3], *Rita Gutiérrez*[3]

[1]Department of Signal Theory and Communications, Universitat Politècnica de Catalunya –
UPC Campus Nord D4-016, E-08034 Barcelona, Spain & IEEC/CRAE-UPC
Tel: +34 934054153, Fax: +34 934017232, E-mail: camps@tsc.upc.edu
[2]SMOS Barcelona Expert Center, Institut de Ciencies del Mar, CMIMA – CSIC, Dept. Physical
Oceanography, Passeig Maritim, 37-49, E-08003 Barcelona
Tel: +34 93 230 95 12/00, Fax: +34 93 230 95 55, E-mail: gourrion@cmima.csic.es
[3]DEIMOS ENGENHARIA, Av. D. João II, Lote 1.17, Torre Zen, 10º, 1998-023 Lisboa, Portugal,
Tel: +351 21 893 3013 Fax: +351 21 896 9099 E-mail: antonio.gutierrez@deimos.com.pt

ABSTRACT

SMOS imagery has been analyzed to study: 1) radio-frequency interference (RFI) detection and mitigation algorithms, and 2) the statistical properties of RFI. Results show that with a high probability of detection (~0.75), the probability of false alarm is high as well (~0.68), and most snap-shots seem to be contaminated, even though the estimated RFI value is weak, and the impact in the SMOS imagery may not be even noticeable. Results of the detection and mitigation algorithm are presented, with the statistical analysis of more than 13000 L1b snap-shots.

Index Terms—RFI, SMOS, probability of detection, probability of false alarm.

1. INTRODUCTION

The European Space Agency mission SMOS was successfully launched on November 2nd, 2009. Its main objectives are the determination of Soil Moisture over land [1] and Sea Surface Salinity over the oceans [2], with an accuracy of 0.04 m^3/m^3 every 3 days with a spatial resolution of 50 km [3, R-4.6.1-002 to 004] at level 2, and 0.1 psu every 10 days with a spatial resolution of 200 km [3, G-4.7.2-005] at level 3. Unfortunately, the first SMOS images [4] using data from the on-ground Image Validation Tests showed a large amount of RFI, specially over land in Europe and Asia, but in some small areas of Africa and Greenland as well (Fig. 1). A refined analysis using on-board calibration data allowed to focus the brightness temperature images [5], but even though the RFI regions became more localized, the amount of RFI was in many occasions so large, that the tails of the "impulse response" to a RFI quasi point source extended over the whole image, making difficult the retrieval of geophysical parameters, mainly over land, but not exclusively (Fig. 2).
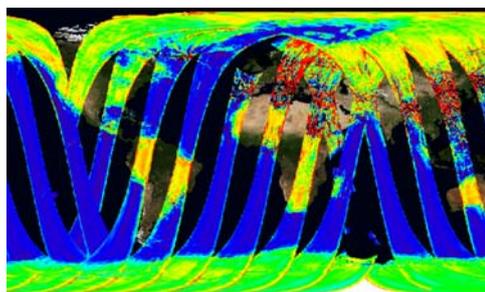

Figure 1. First data (uncalibrated) sent to Earth by the MIRAS instrument on ESA's SMOS satellite [4].
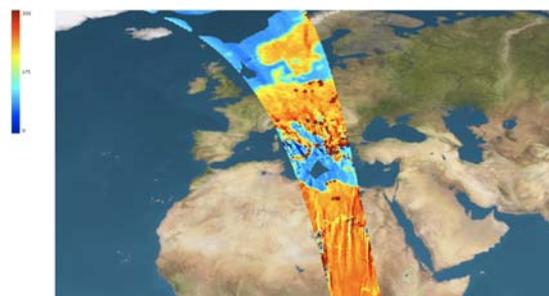
Fig. 2. First image after in-orbit calibration

In [6] an analysis of the potential sources of RFI and their impact was performed, it included: 1) nearby emissions from L-band radars, non-GSO and GSO MSS, 2) harmonics of lower frequency emissions, and 3) possible jamming, which may or may not be deliberately generated. From all the possible interferences, the most important ones were predicted to be those generated by L-band radars due to the high levels of transmitted power, which may interfere in an area of 80 km x 700 km (error 10^{-2} in the normalized cross-correlations) and non-GSO MSS (non Geo-Stationary Orbit Mobile Satellite Services) up-link transmitters (due to the

low spurious rejection and to their proximity to the 1400–1427 MHz band), which may interfere in an area of 50 km x 92 km (error 10^{-2} in the normalized cross-correlations).

However, the fact that Europe and North of Asia are the regions most affected by RFI, while Regions 2 and 3 are generally clean, seems to indicate that fixed and mobile services (assigned in this band too, but only in Region 1), may be more important than radio-localization services (assigned in all three Regions) [7, 8].

First of all, a number of typical RFI scenarios are presented in Section 2. In Section 3 a RFI detection and mitigation algorithm that has been implemented on L1b SMOS data is briefly described. Finally, Section 4 presents the statistical analysis performed on more than 13000 snap-shots.

2. TYPICAL SMOS RFI SCENARIOS

At the time of writing this document more than 13000 snap-shots had been analyzed corresponding to the March 3rd, 2010. Figures 3-6 show different typical RFI scenarios. The left panels are the SMOS L1b data. The central panels are the RFI-cleaned SMOS L1b data. The right panels are the estimated RFI map, the one that is subtracted to the left panel to get the central one. Solid lines correspond to the Earth-sky horizon and its aliases, while dashed lines to the unit circle and its aliases. Plots (a) and (c) correspond to Y-polarization, while (b) and (d) to X-polarization, acquired consecutively every 1.2 s in dual-polarization mode. The exact name of the SMOS data file is shown in the figure title. Figures 3-5 show a typical behavior in which RFI sources appear in the Earth-sky horizon (solid lines) and have a very well defined polarization characteristics, since RFI sources are stronger at Y-polarization, than at X-polarization, which in this part of the field of view (FOV) roughly corresponds to vertical and horizontal polarizations, respectively. It is worth noting that they are not constant in amplitude (Figs. 4a and 4c, and Figs. 5a and 5c, and 5b and 5d). In some cases (Fig. 4c) RFI is so strong that completely corrupts the whole brightness temperature (BT) image, not only appearing as a strong point source, but probably corrupting the denormalization coefficients of the visibility samples as well.

Figure 3. RFI scenario 1: polarization-dependent behavior of RFI sources.

Figure 4. RFI scenario 2: polarization- and time-dependent behavior of RFI sources, present mostly at Y-pol (*a* and *c*). RFI in *c* completely corrupts the BT image.

Figure 5. RFI scenario 3: Same as Fig. 4. Note how some RFI sources are disappear from *a* to *c*, and from *b* to *d*, while others appear or become stronger.

Figure 6. RFI scenario 4: tens of RFI sources in the whole BT image (full hexagon, including alias regions).

3. SMOS-TAILORED RFI DETECTION AND MITIGATION ALGORITHM

As it can be appreciated in Figs. 3-6, most RFI sources appear as point sources to instrument's angular resolution. Therefore, the proposed algorithm (still under refinement) takes advantage of previous techniques develop in the frame of the SMOS mission:

1. BT pixels larger than a given threshold (e.g. 310 K) are flagged as potentially corrupted.
2. Following the same concept of the Sun cancellation algorithm derived in [9], applied recursively as in the CLEAN algorithm [10] to all the BT pixels found in #1, the strongest RFI sources are located and cancelled. The main problems in this case are:
   a. As opposed to the Sun, the exact location of the RFI sources is not known, and the accuracy of the estimation is limited by the step of the (ξ, η) grid (64 x 64 in the SMOS official processor).
   b. Due to the (usually) lower values of the equivalent BT values of the RFI sources, as compared to the Sun, the background BT estimation becomes more critical, and
   c. Background BT estimation is more difficult, since RFI sources tend to be in coastal regions (surrounded by land and sea)
3. In the remaining BT image, the background image is subtracted, which is computed as the low-pass filtered BT image with a disk of 6 pixels radius.
4. In the differential image (step 3), pixels with values larger than 0, for which the original BT value is also larger than 60 K (lowest BT value of the sea at H-pol) are considered as potential RFI sources.
5. The regions in #4 for which $4 \cdot \pi \cdot \text{area}/\text{perimeter}^2$ is larger than 0.2, and smaller than 4, are considered as "round" RFI regions (ideally this metric should be equal to 1, but due to discretization of the (ξ, η) grid these range of values has been empirically enlarged).
6. For regions in #5, the procedure as in #2 is applied.

4. STATISTICAL STUDY OF SMOS RFI

The RFI number and intensity vs. snap-shot number is shown in Fig. 7. As it can be appreciated, nearly all snap-shots exhibit some degree of RFI, even a few sources of a few hundred Kelvin, as those in the snap-shots 2000-2200, 2400-2600 or 3000-3400. At this point it is worth to note that many of the detected potential RFI sources are actually false alarms induced by the thermal noise and the low detection threshold set to increase the probability of detection (see Figs. 3-6, right panels). The histogram of estimated RFI values is shown in Fig. 8a, while Fig. 8b shows the cumulative distribution function of the fraction of snap-shots having RFI sources smaller than the abscissa: 10% have $T_{\text{interference}} < 145$ K, and 50% have $T_{\text{interference}} < 549$ K.

a)
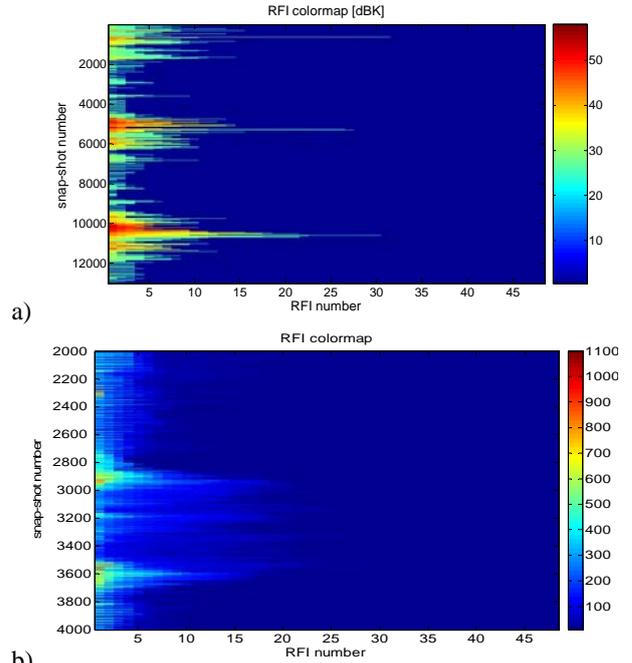
b)

Figure 7. RFI number and intensity vs. snap-shot number: a) 13011 snap-shots analyzed log scale ($10 \cdot \log_{10}(T_{[K]})$, b) zoom of (a) in the "quiet zone" between snap-shots 2000 and 4000 in linear units.

a)
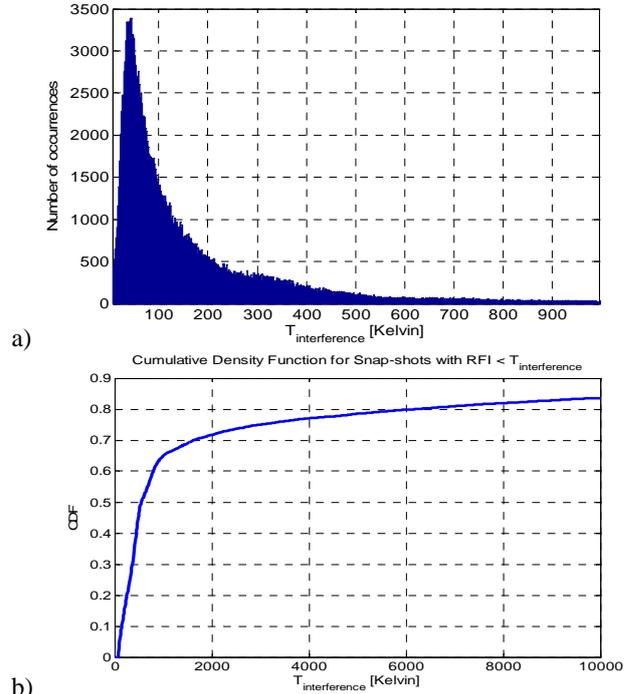
b)

Figure 8. a) Histogram of estimated RFI values (in 2 K bins, truncated up to 1000 K). Mean value = 166 K, standard deviation = 242 K, most probable value = 40-45 K bins, maximum value = $6.9 \cdot 10^5$ K. b) Cumulative density function of snap-shots having RFI sources smaller than the abscissa.

Finally, Fig. 9a shows the histograms of number of RFI sources per snap-shot. The blue histogram includes all detected RFI sources and exhibits a bimodal distribution, with peaks around 5 and 25 RFI sources per snap-shot. It is worth to note that according to this estimation there are not RFI-free snap-shots, which is highly unlikely. If only the estimated RFI sources larger than 150 K were retained (note the large number of very weak estimated RFI sources in Figs. 3-6 due to the presence of noise), then the distribution would have a peak at zero (~10% of the snap-shots), then peaks around 3-4 sources per snap-shot, and finally decreases monotonically, as expected.

Figure 9b shows the corresponding cumulative density function for both histograms, that provides a quantitative view of the number of RFI sources in the SMOS snap-shots.

a)

b)
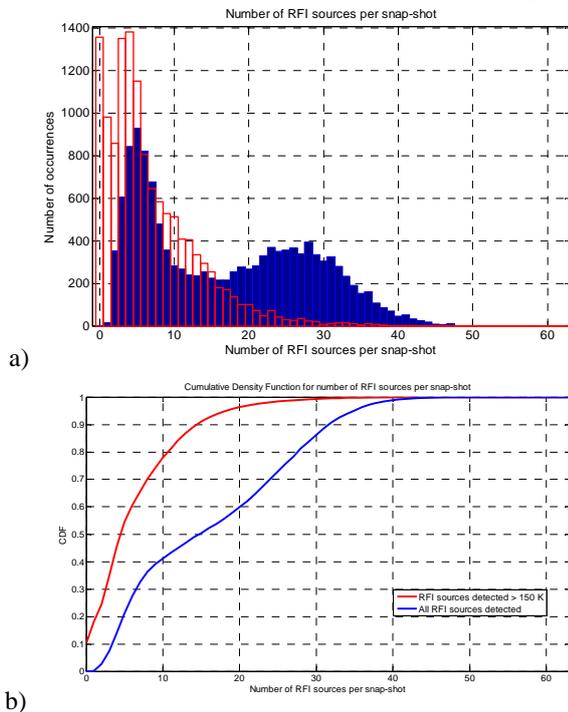
Figure 9. Number of RFI sources per snap-shot a) histogram and b) cumulative density function: all detected RFI sources (blue), and RFI sources stronger than 150 K only (red).

Finally, the probability of Detection (P_d) and False Alarm (P_{fa}) has been estimated by visual inspection of 50 SMOS L1b snap-shots (as in Fig. 3a left), and the processed ones (as in Fig. 3a center and right). Including RFI-free ocean-only snap-shots for which the algorithm described in Section 3 has found some RFI sources (due to the noise structure in the L1b image), the $P_d = 0.47$, and the $P_{fa} = 0.79$. Excluding the RFI-free ocean-only snap-shots the probability of detection increases up to $P_d = 0.75$, and the probability of False Alarm decreases down to $P_{fa} = 0.68$, which is still very large. However, the impact in the RFI-mitigated L1b SMOS images is not as important as one

would expect, since for most of the false alarms, the estimated RFI value is very small.

6. CONCLUSIONS

This manuscript has presented the problems associated to the presence of RFI in SMOS imagery (L-band, 1.4 GHz), as well as its polarization and time dependence. An algorithm has implemented to operate directly with L1b SMOS data only, so that it can be inserted without problems in the SMOS operational processing chain. Statistical analysis of more than 13000 snap-shots has shown that on average there are 3-4 RFI sources per snap-shot (including only those larger than 150 K), with a mean value of 166 K, with a standard deviation of 242 K, and a most probable value 40-45 K, even though values as high as $6.9 \cdot 10^5$ K can be reached. More snap-shots are under analysis to improve the representativeness of this anaylisis to all regions in the world.

12. REFERENCES

[1] Kerr, Y.H., P. Waldteufel, J.P. Wigneron, S. Delwart, F. Cabot, J. Boutin, M.J. Escorihuela, J. Font, N. Reul,C. Gruhier, S. Enache-Juglea, M. R. Drinkwater, A. Hahne, M. Martín-Neira, and S. Mecklenburg, *The SMOS Mission: New Tool for Monitoring Key Elements of the GlobalWater Cycle*, Proceedings of the IEEE, Vol. 98, No. 5, May 2010, pp. 666-687

[2] Font, J., A. Camps, A. Borges, M. Martín-Neira, J. Boutin, N. Reul, Y.H. Kerr, A. Hahne, and S. Mecklenburg, *SMOS: The Challenging Sea Surface Salinity Measurement From Space*, Proceedings of the IEEE, Vol. 98, No. 5, May 2010, pp. 649-665

[3] SMOS System Requirements Document, doc. SO-RS-ESA-SYS-0555, issue 4.1, date 28-09-2004. http://eopi.esa.int/

[4]http://www.esa.int/esaLP/SEMOOU49J2G_LPsmos_1.html#subhead1

[5] http://www.smos-bec.icm.csic.es/node/36

[6] Camps, A., I. Corbella, F. Torres, J. Bará, and J. Capdevila, *RF Interference Analysis in Aperture Synthesis Interferometric Radiometers: Application to L-Band MIRAS Instrument*, IEEE Transactions on Geoscience and Remote Sensing, Vol. 38, No. 2, March 2000, pp. 942-950.

[7]http://www.mityc.es/telecomunicaciones/Espectro/CNAF/4atribuciones.pdf

[8]http://www.mityc.es/telecomunicaciones/Espectro/CNAF/3notasrr.pdf

[9] *A. Camps, M. Vall-llossera, N. Duffo, M. Zapata, I. Corbella, F. Torres, V. Barrena, Sun Effects In 2D Aperture Synthesis Radiometry Imaging And Their Cancellation,* IEEE Geoscience and Remote Sensing Letters, Vol. 42 (6), pp. 1161-1167, June 2004

[10] Högborn, J. A., *Aperture synthesis with non-regular distribution of interferometer baselines*, Astron. Astrophys. Suppl., Vol. l5, pp. 417–426, 1974.